Measurement of the asymmetry parameter A in $\pi^- p$ elastic and charge-exchange scattering at pion energies $T_\pi = 98$, 238, 292, and 310 MeV

J. C. Alder,* C. Joseph, J. P. Perroud, and M. T. Tran
Institut de Physique Nucléaire de l'Université de Lausanne, CH-1015 Lausanne, Switzerland

G. H. Eaton,† R. Frosch, H. Hirschmann,‡ S. Mango, J. W. McCulloch,§ and P. Shrager
SIN, Swiss Institute for Nuclear Research, CH-5234 Villigen, Switzerland

G. Strassner|| and P. Truöl
Physik-Institut der Universität Zürich, CH-8001 Zurich, Switzerland

P. Weymuth and P. Wiederkehr
Laboratorium für Hochenergiephysik der Eidgenossische Technische Hochschule Zürich, CH-5234 Villigen, Switzerland

(Received 28 October 1981)

The asymmetry parameter A in $\pi^- p$ elastic scattering at incident pion laboratory kinetic energies T_π of 98, 238, and 292 MeV and in $\pi^- p$ charge-exchange scattering $\pi^- p \to \pi^0 n$ at $T_\pi = 238$, 292, and 310 MeV have been measured over a wide range of scattering angles (typically from about 60° to 130° c.m.) with a polarized proton target. The data have been used in an energy-independent phase-shift analysis to improve the precision of the pion-nucleon phase shifts, to set new limits on violation of isospin conservation in the pion-nucleon S wave, and to confirm significant charge dependence in the $P_{3/2}$ wave.

I. INTRODUCTION

The measurements of the asymmetry parameter A (or analyzing power A) in $\pi^- p$ elastic and charge-exchange scattering to be discussed here are part of an extensive experimental study[1–4] of pion-nucleon polarization effects at the Swiss Institute for Nuclear Research (SIN) in the incident pion laboratory energy range between 98 and 310 MeV. If parity invariance holds, the asymmetry parameter A is equal to the polarization parameter P.

The main goal of the first part of the experiment, concerning elastic $\pi^- p$ scattering, was to improve the precision of the pion-nucleon phase shifts, particularly the S_{11}, P_{11}, P_{33}, D_{13}, and D_{15} phase shifts. In their analysis Carter, Bugg, and Carter[5] have found that a strong correlation exists between the best-fit values of the $P_{33}(\pi^- p)$, P_{11}, and S_{11} phase shifts above the resonance pion energy if only cross sections are considered, and that a precise determination of these phase shifts requires the inclusion of polarization data. The earlier SIN measurements of the analyzing power A in $\pi^+ p \to \pi^+ p$ and $\pi^- p \to \pi^- p$ (the latter at energies of 291 and 308 MeV) have already been included in the recent phase-shift analyses of Koch and Pietarinen[6] and of Zidell, Arndt, and Roper.[7] This work improves the precision and extends the energy range of these polarization measurements.

The second part of the experiment, consisting of the first extensive measurements of $\pi^- p$ charge-exchange asymmetry in this energy region, was aimed mainly at improving the tests of isospin invariance in the pion-nucleon (πN) interaction. A breakdown of isospin invariance would manifest itself either by nonzero transition matrix elements $\langle I', I_3 \mid T \mid I, I_3 \rangle$ where the total isospin I' of the final πN state differs from the total isospin I of the initial πN state or through a dependence of the matrix element $\langle I, I_3 \mid T \mid I, I_3 \rangle$ on the third component I_3 of the isospin.

In their 1973 πN phase-shift analysis, Laurikainen and Törnqvist[8] have expressed isospin nonconservation by the mixing parameters $\omega_{I\pm}$ (cf. Appendix A), which are zero if isospin is conserved. It was found that $\omega_{I\pm}$ was not consistent with zero in the S wave; at incident pion laboratory energies T_π of 300 and 581 MeV the parameter ω_0 was found to differ from zero by about five standard deviations. Furthermore, simpler comparisons[9,10] checking the triangle inequality

$$[(\sigma^+)^{1/2}-(\sigma^-)^{1/2}]^2 \leq 2\sigma^0 \leq [(\sigma^+)^{1/2}+(\sigma^-)^{1/2}]^2 \quad (1)$$

deduced from $\sqrt{2}a^0=a^+-a^-$ (assuming $\omega_{I\pm}=0$ for all I; notation cf. Appendix A) indicated a violation of isospin conservation near 180° for some experimental data in the same energy region.

The results of Refs. 8 and 9 cannot, however, be considered as good evidence for isospin nonconservation: allowing ω_0 and the phase-shift difference $\Delta_0=\delta(S_{31},\pi^+p)-\delta(S_{31},\pi^-p)$ (cf. Appendix A) to differ from zero only improves the χ^2 value in the analysis of Ref. 8 from 294 to 265 for 160 degrees of freedom at $T_\pi=300$ MeV, and from 402 to 262 for 136 degrees of freedom at $T_\pi=581$ MeV.

The observations of Refs. 8 and 9 prompted two groups at UCLA (Refs. 11 and 12) and CERN (Ref. 13) to initiate new series of charge-exchange differential-cross-section measurements. Their results appear consistent with the triangle inequality [cf. Eq. (1)]. The CERN group has also analyzed their data in terms of ω_0, using the Carter, Bugg, and Carter phase shifts. Their results in the first resonance region ($120<T_\pi<250$ MeV) are consistent with $\omega_0=0$ within errors, typically ± 0.05. At these energies, the P_{33} resonance dominates the charge-exchange cross sections, so that they are not very sensitive to ω_0. An improvement is expected from measurements of the asymmetry parameter A^0 in $\pi^- p$ charge-exchange scattering. For instance, at $T_\pi=310$ MeV and $\theta_{\text{c.m.}}=110°$, a change in ω_0 from 0 to 0.1 rad leads to a change of 0.1 in the calculated value of A^0.

Carter, Bugg, and Carter,[5] and later Pedroni *et al.*[14], have looked for an effect of charge-independence violation, namely for mass and width differences between the doubly positive state Δ^{++} and the neutral state Δ^0 of the first P_{33} resonance. The $\pi^+ p$ total-cross-section data of Refs. 5 and 14 indicate that both the mass and the width of the Δ^{++} are smaller than those of the Δ^0 by a few MeV even after electromagnetic corrections have been applied to the experimental data. The order of magnitude of the observed (Δ^0,Δ^{++}) mass and width differences agree with various theoretical estimates.[7] In some of the recent phase-shift analyses this charge dependence has been taken into account by allowing the phase shift $\delta^{++}(P_{33})$ for $\pi^+ p$ scattering to differ from $\delta^0(P_{33})$ for the neutral channel, i.e., for both $\pi^- p$ elastic and $\pi^- p$ charge-exchange scattering. In these analyses, "hadronic" phase shifts are calculated, i.e., phase shifts describing the strong interaction of the pion and the nucleon. In the 1980 phase-shift analysis of Koch and Pietarinen,[6] based on differential cross sections and polarizations including the SIN $\pi^+ p$ asymmetry data[1–3] and some of the SIN $\pi^- p$ asymmetry data,[4] no significant differences $\delta^{++}(P_{33})-\delta^0(P_{33})$ were found. However, in the 1973 analysis of Carter, Bugg, and Carter,[5] despite the fact that only few A-parameter data were available, the difference $\delta^{++}(P_{33})-\delta^0(P_{33})$ was found to be $(2.5\pm 1.1)°$ and $(1.86\pm 0.64)°$ at $T_\pi=263.7$ and 291.6 MeV, respectively, by including total cross sections and using theoretical values of the D phases.

The A-parameter measurements can contribute significant additional evidence for the charge dependence of the $\delta(P_{33})$ phase. In the phase-shift analyses without A parameters, there are strong correlations between the resulting phase shifts, e.g.,[5] between $\delta^0(P_{33})$ and other phase shifts. These correlations are reduced by the inclusion of A-parameter data in the phase-shift analysis, and thus the precision of all involved phase shifts including that of $\delta^0(P_{33})$ is improved.

II. EXPERIMENTAL METHOD

Elastic and charge-exchange asymmetry measurements were carried out in the $\pi M3$ pion channel[15] at SIN using a polarized proton target. The beam momentum was determined from magnetic-field maps of the bending magnets of the channel and checked by measuring range curves for the protons transmitted through the channel operating in positive-particle mode; the mean beam momentum was by this method known to a precision of 0.4%.

The apparatus used for the elastic-scattering measurements is shown in Fig. 1. The polarized target consisted of a 1-cm^3 volume of butanol pellets, which were ^{3}He cooled at 0.5 K and placed in a 2.5-T magnetic field generated by superconducting Helmholtz coils. By the dynamical method, polarizations of typically 60% were obtained. The target polarization was measured continuously by a fast-sweep NMR system with a total uncertainty $\Delta P_T/P_T$ of $\pm 4\%$ (one standard deviation).[16]

Incoming pions from the $\pi M3$ channel [typical intensity 2.10^6 π^-/sec at 310 MeV for a momentum bite $\Delta p_\pi/p_\pi$ of 4% full width at half maximum (FWHM)] were detected in scintillation counters S_1 and S_2 and in a silicon surface barrier detector Si (active area: 0.64 cm^2) placed in front of the butanol target (see Fig. 1). Scattered pions were detected in counters π_5 or π_6 and in one of the set of counters π_1–π_4, while scattered protons were registered in P_1 or P_2. The counters π_5, π_6, P_1, and P_2 were identical $100\times 10\times 5$ cm^3 plastic scintillator bars at 60 cm from the target and viewed by 56 DVP photomultiplier tubes at both ends. The counters π_1–π_4 were $4\times 4\times 0.3$ cm^3 plastic scintillators and were used in

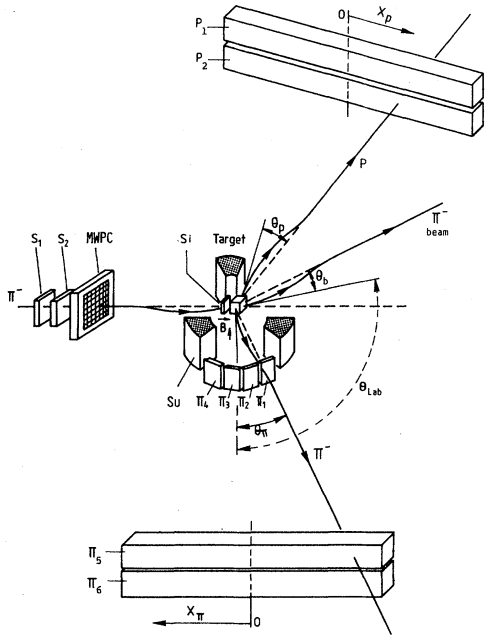

FIG. 1. Diagram of the apparatus used for the measurement of the asymmetry parameter in $\pi^- p$ elastic scattering (not to scale). S_1, S_2, π_i, P_i: scintillators; centers of π_5, π_6, P_1, and P_2 are 0.6 m from target; the counter π_5 was placed on top of π_6, as was P_1 on P_2. Si: silicon surface barrier detector (active area: 0.8×0.8 cm^2, thickness: 1.4 mm). T: polarized proton target. $\vec{B}$: direction of the magnetic field. MWPC: multiwire proportional chamber (beam-profile monitor). Su: supports of the superconducting Helmholtz coils.

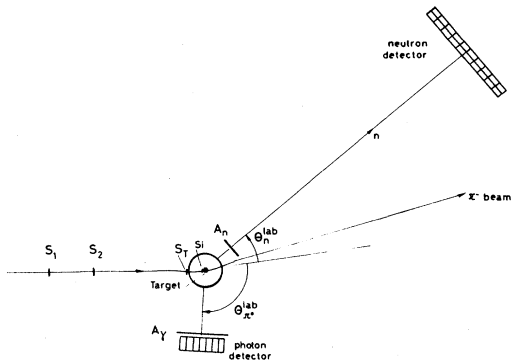

FIG. 2. Apparatus used for the measurement of the asymmetry parameter in $\pi^- p$ charge-exchange scattering (top view) A_n, A_γ: charged-particles veto counters; S_1, S_2: see Fig. 1. Si: silicon surface barrier detector (active area: 1.5×1.5 cm^2). For the runs at 237 and 292 MeV, this silicon detector was not available and was replaced by a $1.5 \times 1.5 \times 0.2$-cm^3 scintillator S_T located 15 cm upstream of the target. Neutron detector is 3 m from target; photon detector is 0.6 m from target.

coincidence with the π_5—π_6 scintillator bars. The times of the two signals generated by a charged particle hitting a scintillator bar were registered; this allowed a time-of-flight (TOF) resolution of 700 psec FWHM and a spatial resolution along the scintillator bar of 3.5 cm FWHM. The start signal for the TOF measurements for the pion and proton counters was generated from the counter S_2 in the pion beam. In addition to the TOF measurement for each event, pulse-height information from the scintillator bars was also recorded allowing clear separation between pions and protons. Details of the electronic configuration are contained in Ref. 15.

The experimental arrangement used for the charge-exchange asymmetry measurements is shown in Fig. 2. The volume of the polarized target in this case was increased to 8 cm^3 and the Helmholtz coils were modified accordingly. Except for the 310-MeV runs, the silicon surface barrier detector shown in Fig. 2 was not available and was replaced by a small scintillator S_T ($1.5 \times 1.5 \times 0.2$ cm^3) 15 cm upstream of the target and outside the target assembly.[17] The time of flight and the direction of the outgoing neutron were measured with 20 scintillator bars similar to those previously described. Coincident photons from π^0 decay were registered by a photon detector array of 49 (7×7) lead glass blocks ($5.5 \times 5.1 \times 11$ cm^3, 7 radiation lengths, standard nuclear lead glass from St. Gobain), viewed by Philips XP1010 photomultiplier tubes. This photon detector, located at 60 cm from the target, subtended a solid angle of 0.366 sr and was essential to reduce the quasielastic background from protons bound in nuclei of the butanol target. Anticoincidence counters A_γ and A_n were used to veto charged particles entering the photon detector and the neutron counter array. The electronics will be described in Ref. 17. In both experiments, a PDP 11/34 on-line computer interfaced via CAMAC was used for data collection and control.

For both experiments, the polarization of the target was in the vertical direction and the central scattering plane was horizontal. For the idealized geometry, in which the target polarization and the scattering plane are exactly perpendicular to each other, the counting rate $n(\theta_{\text{c.m.}}, P_T)$ of good events from polarized protons is given by the expression

$$n(\theta_{\text{c.m.}}, P_T) = n_0(\theta_{\text{c.m.}})[1 + A(\theta_{\text{c.m.}})P_T] , \qquad (2)$$

where $\theta_{\text{c.m.}}$ is the scattering angle in the center-of-mass system, $A(\theta_{\text{c.m.}})$ is the asymmetry parameter (A parameter), and P_T is the polarization of the target; $n_0(\theta_{\text{c.m.}})$ is the counting rate for $P_T = 0$. For

the charge-exchange experiment, where the neutron detector covered a large azimuthal acceptance, an average value of the effective target polarization had to be used. The corresponding corrections to the value of A amount to 2% in the worst cases.

The A parameter was measured by determining at fixed incoming pion energy and scattering angle, the counting rate for up and down polarization of the target; the target polarization was reversed by slightly changing the applied microwave frequency.[16]

III. DETERMINATION OF THE A PARAMETER

According to Eq. (2), the rate of scattered pions detected at a fixed angle depends linearly upon the target polarization. Therefore, the A parameter is obtained directly by a numerical fit of a straight line to the relevant event rate measured at different values of the target polarization P_T, i.e., typically three data points near $P_T = +0.6$ and three points near $P_T = -0.6$ at each setting of T_π and $\theta_{\text{c.m.}}$. As P_T was in all cases close to either $+0.6$ or -0.6, our fit did not yield a restrictive test of the linear relation predicted from Eq. (2). The relevant event rates are those corresponding to elastic $\pi^- p$ and charge-exchange $\pi^- p$ scattering once backgrounds have been subtracted from the data. The most significant backgrounds in both experiments were quasielastic and inelastic scattering of pions from the carbon nuclei in the butanol, and also from other materials of the target, such as the ^{3}He coolant and the windows.

A. Extraction of events from background in the $\pi^- p \to \pi^- p$ experiment

The method of extracting good events from background in the elastic-scattering experiment can be understood by referring to Figs. 3 and 4. Figure 3 shows the time of flight of the particle detected in the proton arm (counter P_1 or P_2) plotted against the position of the coincident particle detected in the pion arm (π_5 or π_6). The upper band is due to elastic pion scattering from free protons and is separated from a band due to events in which fast particles are detected in both arms. In Fig. 4 the position of the "proton", x_p, is plotted against the position of the "pion" x_π. Projections (Fig. 5) on the x_p axis for 5-cm-wide x_π slices of Fig. 4 show that the background beneath the good events after TOF and pulse-height cuts is quite small (ranging from 7 to 23%); it was evaluated by interpolation, assuming a polynomial form of the background; this assumption was verified by direct background measurements.[15] The uncertainty of the analyzing power A due to this background subtraction was in all cases a small contribution to the total uncertainty of A, which was mainly due to counting statistics and to the uncertainty of the target polarization.

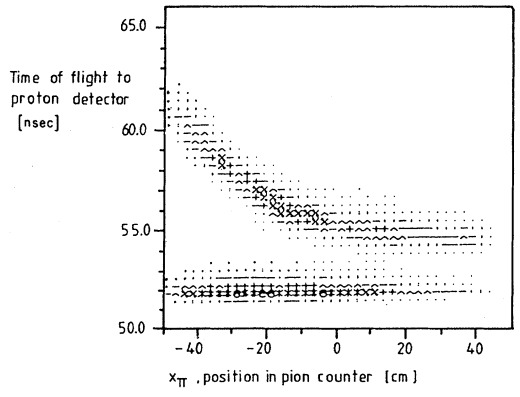

FIG. 3. Time of flight of the particle detected in one of the proton bars versus the position of the coincident particle in the pion bar (x_π). The zero of the ordinate is arbitrary.

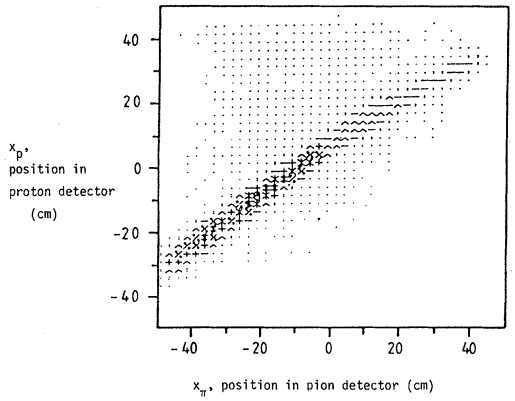

FIG. 4. As in Fig. 3, but showing the position of the two outgoing particles of each event in the pion and proton bars, respectively.

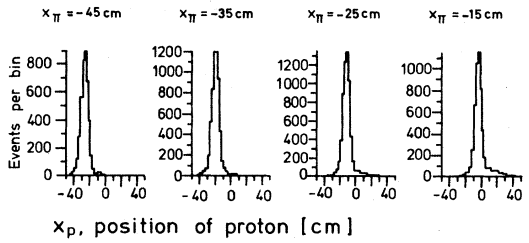

FIG. 5. Projections of Fig. 4 (raw data) onto the x_p (position of proton) axis for 5-cm-wide bins in x_π (position of the pion). Time-of-flight and pulse-height cuts have been applied to the raw data. The TOF cuts select the kinematical locus of Fig. 3. Pulse-height cuts select a pion and a proton in the counters $\pi_5\pi_6$ and P_1, P_2, respectively.

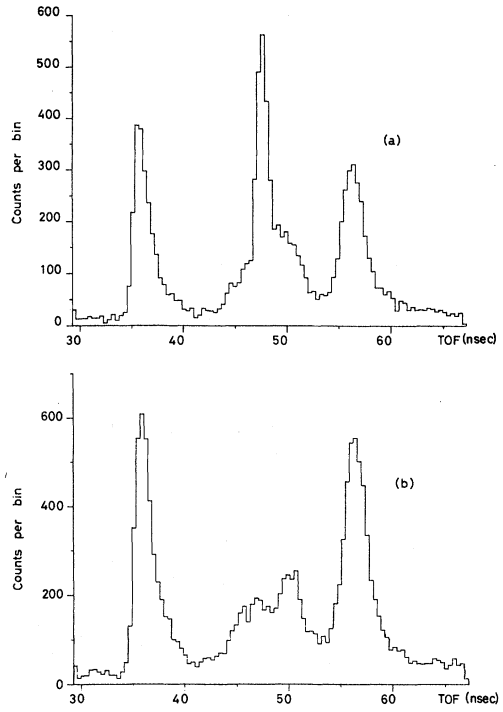

FIG. 6. Time-of-flight spectra registered at $T_\pi = 237$ MeV and $\theta_{c.m.} = 126.1°$ in the $\pi^- p$ charge-exchange experiment for (a) the polarized butanol target and (b) the dummy carbon target. The peak at 51 nsec in (b) is attributed to neutrons from charge exchange off free protons of the scintillator S_T. Since this scintillator was placed in front of the target assembly, the π^- beam was not yet bent and the laboratory neutron scattering angle was in this case 10° larger than the angle of the neutrons scattered from the target, resulting in a larger time of flight. The normalization factor, i.e., the ratio between the butanol-run and the dummy-target-run beam fluxes, was 0.57 and was not taken into account in (b).

B. Extraction of events from background in the $\pi^- p$ charge-exchange experiment

Charge-exchange scattering of the pions off free protons of the polarized target is identified by the TOF of the neutrons to the neutron detector. The calibration of the time-to-digital converters (TDC's) associated with each neutron detector was checked by placing the neutron detectors into the pion beam at reduced intensity. An additional check of the TDC calibration was done using events in which a neutron detector registered one of the photons from π^0 decay. An example of a TOF distribution for one of the neutron counters is shown in Fig. 6(a), where a narrow peak at 48 nsec, due to neutrons from charge exchange with free protons, is superimposed on a broader peak due to neutrons from charge exchange with other target nuclei. The peak at 36 nsec is attributed to photons from the decay of a π^0 of an event satisfying the trigger conditions. The peak at 57 nsec is due to photons created in or near the target from the subsequent beam burst, about 20 nsec after the burst which produced the trigger. The background, assumed to be polarization independent, was measured substituting the butanol of the polarized target with a dummy target consisting of a

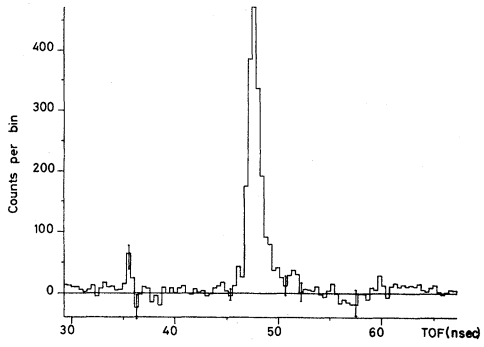

FIG. 7. As in Fig. 6, but with normalized dummy-target data removed from the raw time-of-flight spectrum.

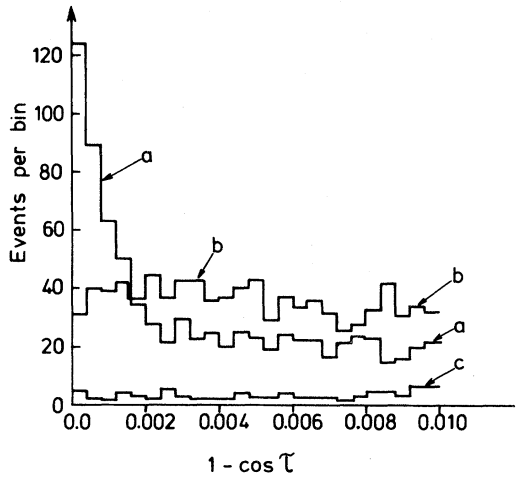

FIG. 8. Extraction of radiative-pion-capture events $\pi^- p \to \gamma n$ at $T_\pi = 310$ MeV. Abscissa: $(1-\cos\tau)$, where τ is the c.m. angle between the measured neutron direction and that calculated using $\pi^- p \to \gamma n$ kinematics and the observed photon direction. Ordinate: number of events per bin. Histogram *a*: events with $-1.0 < \Delta t \leq +0.8$ nsec, where Δt is the difference between the measured flight time and that expected for the $\pi^- p \to \gamma n$ reaction. The peak at $(1-\cos\tau) < 0.002$ is attributed to radiative capture on free protons. Histogram *b*: events with $0.8 < \Delta t < 1.7$ nsec, i.e., charge-exchange events only. Histogram *c*: events registered with the dummy target for $-1.0 < \Delta t < 1.7$ nsec.

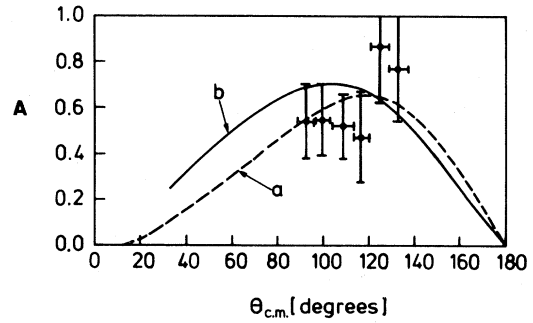

FIG. 9. Comparison of our measured values of the analyzing power for $\pi^- p \to \gamma n$ with predictions derived from analyses of photoproduction data. Abscissa: c.m. angle between pion and photon momenta. Ordinate: analyzing power for $\pi^- p \to \gamma n$. Points with error bars: our measured values for $T_\pi = 310$ MeV (total c.m. energy $\sqrt{s} = 1320$ MeV). Curves: predictions for the recoil-nucleon polarization in $\gamma n \to \pi^- p$ at $\sqrt{s} = 1315$ MeV. Curve a: Ref. 18; curve b: Ref. 19.

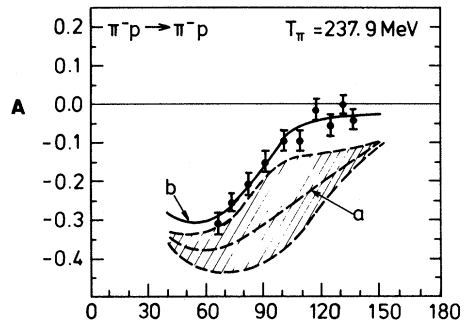

FIG. 11. As in Fig. 10, but for $T_\pi = 237.9$ MeV. Curve a is derived from the phase shifts of Ref. 5. The sensitivity of the predicted values of the asymmetry parameter to the S_{11} phase is indicated by the shaded area, which shows the amount of variation of the predicted P parameter as the S_{11} phase of Ref. 5 is allowed to vary by its quoted uncertainty. Curve b is derived from our new phase shifts; cf. Table III.

carbon block of the same thickness [Fig. 6(b)]. The dummy-target TOF spectrum was normalized to the beam fluxes of the butanol runs and subtracted from the butanol TOF spectra. The TOF spectrum of Fig. 6(a) after subtraction of the background is shown in Fig. 7. The normalization of the dummy-target data was allowed to vary in a 10% range in order to account for the uncertainty of the filling factor of the polarized target. We estimated the error introduced by this procedure using the two extreme estimates of the dummy-target normalization factor which still gave a spectrum consistent with zero before and after the peak of neutrons scattered off free protons. This error (±5% typically) was added in quadrature to the statistical uncertainty of the area of the good events peak.

For about half of the 310-MeV measurements, dummy-target data were not available. In these cases, the background was determined by a method similar to that used for the elastic $\pi^- p$ measurements, i.e., the quasielastic background was determined by polynomial fitting of the event distributions on either side of the good events peak.

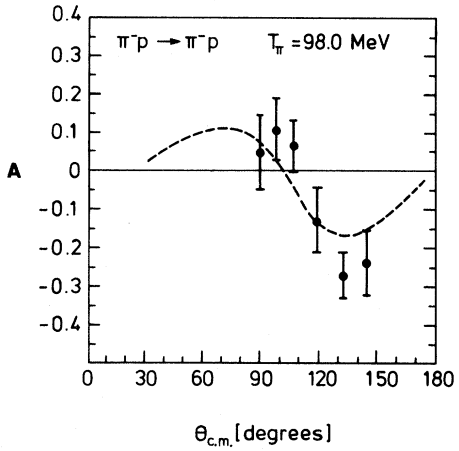

FIG. 10. Asymmetry parameter A in $\pi^- p$ elastic scattering at an incident pion laboratory kinetic energy T_π of 98.0 MeV, versus center-of-mass scattering angle $\theta_{\text{c.m.}}$. Points with error bars: measured values (cf. Table I). Dashed curve is derived from the phase shifts of Ref. 5.

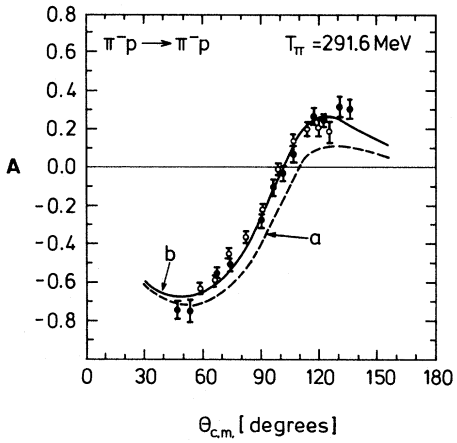

FIG. 12. As in Fig. 10, but for $T_\pi = 291.6$ MeV. Open circles are the results of the present experiment; the full circles are those of previous SIN work (Ref. 4). Curves a and b: cf. Fig. 11.

TABLE I. The asymmetry parameter in $\pi^- p$ elastic scattering at incident pion laboratory kinetic energies of (a) 98.0 MeV, (b) 237.9 MeV, and (c) 291.6 MeV. The quoted errors are the total uncertainties excluding the uncertainties on the target polarization.

c.m. angle (degrees)	Asymmetry parameter A
(a) Mean pion energy 98.0±0.6 MeV	
88.3	0.046±0.096
96.6	0.104±0.079
106.2	0.062±0.065
118.4	−0.132±0.083
132.0	−0.274±0.059
144.1	−0.242±0.083
(b) Mean pion energy 237.9±1.3 MeV	
65.8	−0.313±0.024
73.2	−0.258±0.023
81.5	−0.211±0.026
90.4	−0.153±0.025
99.6	−0.097±0.024
108.6	−0.100±0.024
116.9	−0.017±0.024
124.3	−0.061±0.024
130.6	−0.008±0.023
135.9	−0.047±0.026
(c) Mean pion energy 291.6±1.5 meV	
58.4	−0.630±0.027
65.4	−0.587±0.022
73.3	−0.437±0.022
81.7	−0.363±0.025
90.1	−0.219±0.027
98.4	−0.011±0.029
106.0	0.134±0.034
113.0	0.197±0.032
119.0	0.202±0.044
124.3	0.182±0.055

TABLE II. The asymmetry parameter in $\pi^- p$ charge-exchange scattering at incident pion laboratory kinetic energies of (a) 237.9 MeV, (b) 291.6 MeV, and (c) 310.0 MeV. The quoted errors include all statistical and systemic uncertainties except the error on the target polarization.

c.m. angle (degrees)	Asymmetry parameter A
(a) Mean pion energy 237.9±1.3 MeV	
99.3	0.588±0.055
102.8	0.534±0.048
106.6	0.455±0.049
110.6	0.314±0.046
114.3	0.295±0.046
118.3	0.136±0.040
122.1	0.102±0.041
126.1	0.137±0.040
130.0	0.119±0.044
133.5	0.020±0.047
(b) Mean pion energy 291.6±1.5 MeV	
89.2	0.820±0.035
93.0	0.825±0.034
96.8	0.706±0.034
100.5	0.666±0.035
104.3	0.531±0.040
108.1	0.375±0.032
111.9	0.188±0.032
115.6	0.053±0.035
119.4	−0.134±0.036
123.2	−0.135±0.040
121.6	−0.204±0.066
125.5	−0.205±0.056
129.5	−0.236±0.049
133.4	−0.330±0.050
137.4	−0.331±0.050
141.3	−0.208±0.051
145.3	−0.254±0.055
149.2	−0.284±0.062

C. Background due to radiative pion capture $\pi^- p \to \gamma n$

Radiative-capture events $\pi^- p \to \gamma n$ represent the only polarization-dependent background. Their effect on the charge-exchange asymmetry is of some importance in regions where the asymmetries of the two reactions have opposite sign. A careful removal of these radiative-capture events prior to the determination of the charge-exchange asymmetry is needed. In the kinematical conditions of the charge-exchange experiment, the neutrons from radiative pion capture cannot be distinguished from neutrons due to charge exchange by TOF information alone. However, because radiative capture is a two-body reaction, it can be separated from charge exchange by examination of the angular correlation and coplanarity of the photon and the neutron. This is possible with our apparatus, since both particle directions can be determined with the photon detector array and the neutron detector.

For each event, we calculated, from the measured photon direction, the expected c.m. radiative-capture neutron direction and TOF. The deviation from the

TABLE II. *(Continued).*

c.m. angle (degrees)	Asymmetry parameter A
(c) Mean pion energy 310.0±1.6 MeV	
85.2	0.930±0.053
88.5	0.877±0.052
92.5	0.855±0.043
96.5	0.719±0.059
99.9	0.507±0.059
103.4	0.345±0.061
106.7	0.225±0.062
109.5	0.081±0.057
112.4	−0.049±0.047
114.9	−0.224±0.061
118.2	−0.320±0.055
121.8	−0.327±0.061
125.0	−0.404±0.058
128.3	−0.430±0.060
131.8	−0.419±0.058
135.2	−0.438±0.067
139.4	−0.400±0.053

$\pi^- p \to \gamma n$ kinematics can be measured in terms of 1-cosτ where τ is the c.m. angle between the measured and calculated neutron directions specified above. Events have been split in two groups according to the difference Δt between the measured and calculated neutron time of flight. The first group of events, for which $-1.0 < \Delta t \leq 0.8$ nsec, contains all the $\pi^- p \to \gamma n$ events, and a part of the registered charge exchange and background events, while in the second group ($0.8 < \Delta t < 1.7$ nsec) no radiative-capture event is expected. Figure 8 shows the function 1-cosτ for the two groups of events ($T_\pi = 310$ MeV). The peak at $\tau = 0$ is attribtued to radiative-capture events and its content, once charge exchange has been subtracted by straight-line extrapolation to $\tau = 0$, allowed the determination of the $\pi^- p \to \gamma n$ rate (7% of the charge-exchange rate) and the estimation of the analyzing power for radiative capture. In Fig. 9, this analyzing power is compared to predictions for the recoil nucleon polarization in the inverse reaction $\gamma n \to \pi^- p$ derived from multipole analyses of photoproduction data[18,19] (if time-reversal invariance holds, the above analyzing power and recoil nucleon polarization are equal). At all three energies, the capture rates were used to correct the measured raw charge-exchange rates for the two polarization states of the target; the corrections to the event rate ranged from about 5 to 10%.

IV. EXPERIMENTAL RESULTS

A. Results for the A parameter in elastic $\pi^- p$ scattering

The measured values of the asymmetry parameter in $\pi^- p$ elastic scattering are shown in Figs. 10–12 and listed in Table I. The uncertainties of A given in Table I, and also those in Table II, are due to counting statistics and background subtraction; they do not contain the contribution, due to the target-polarization uncertainty; this contribution, $\Delta A = 0.04A$ in all cases, scales all A values at the same beam energy in the same way. The uncertainty of the mean beam momentum in the center of the polarized target was ±0.4% in all cases.[15] The corresponding uncertainties of the mean incident pion laboratory kinetic energy T_π are given in Tables I and II.

Our new results and the earlier SIN data at 291.5 and 308.0 MeV (cf. Ref. 4) appear to be consistent with each other and with the data of Vasilevsky *et al.*[20] at 300 MeV and with those of Arens *et al.*[21] at 229 and 318 MeV. However, our data and those of Ref. 4 differ significantly from those of Gorn[22] at 243, 247, and 300 MeV, and of Rugge and Vik[23] at 310 MeV. In these comparisons with other data we have assumed a smooth variation of the A parameter with energy.

B. Results for the A parameter in $\pi^- p$ charge exchange

The results for the asymmetry parameter in $\pi^- p$ charge-exchange scattering are shown in Figs. 13–15 and listed in Table II. The only previous measurement of the $\pi^- p$ charge-exchange polarization in our energy region is that of Hill *et al.*[24] at $T_\pi = 310$ MeV and $\theta_{\text{c.m.}} = 30°$. Their data point is outside the angular range of our measurements, so no direct comparison is possible.

V. PHASE-SHIFT ANALYSIS

A. Data summary

We have carried out an energy-independent phase-shift analysis (PSA) of our $\pi^- p$ data together with other pion-nucleon data in the same pion energy region. The laboratory pion energies T_π selected for our PSA were 237.9, 291.6, and 310.0 MeV; they are among the energies chosen in the analysis of Carter, Bugg, and Carter.[5] In addition to the new SIN polarization parameters we used the measurements listed in Table I of the recent PSA paper by Zidell, Arndt, and Roper,[7] i.e., data published since

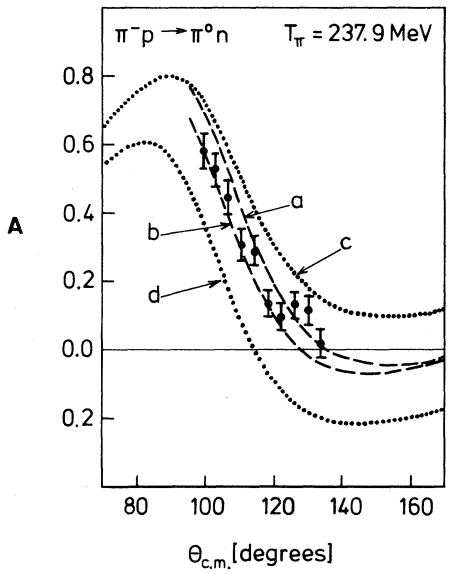

FIG. 13. Asymmetry parameter A in charge-exchange scattering $\pi^- p \to \pi^0 n$ at an incident pion laboratory kinetic energy of 237.9 MeV, versus center-of-mass angle $\theta_{\text{c.m.}}$ between π^- and π^0 momenta. Points with error bars: measured values; cf. Table II. Curve a is derived from phase shifts of Ref. 7 for an S-wave isospin-nonconservation parameter $\omega_0 = -0.1$ rad (cf. Appendix A; all other isospin-nonconservation parameters zero). Curve b: same as curve a, but for $\omega_0 = +0.1$ rad. Curve c: upper "isospin bound" for A (cf. Sec. V G and Appendix B). Curve d: lower isospin bound.

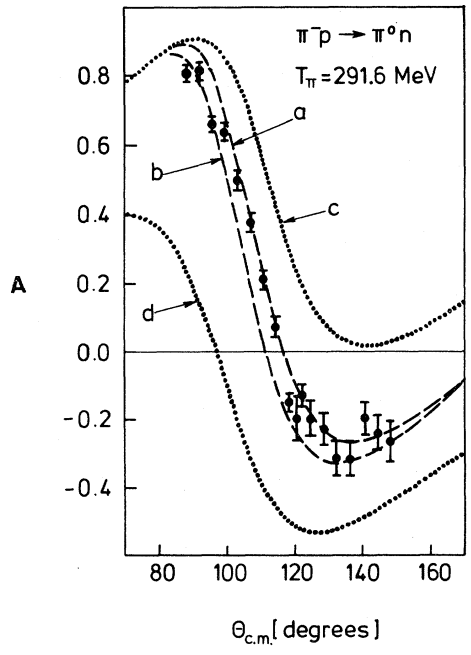

FIG. 14. As in Fig. 13, but for $T_\pi = 291.6$ MeV.

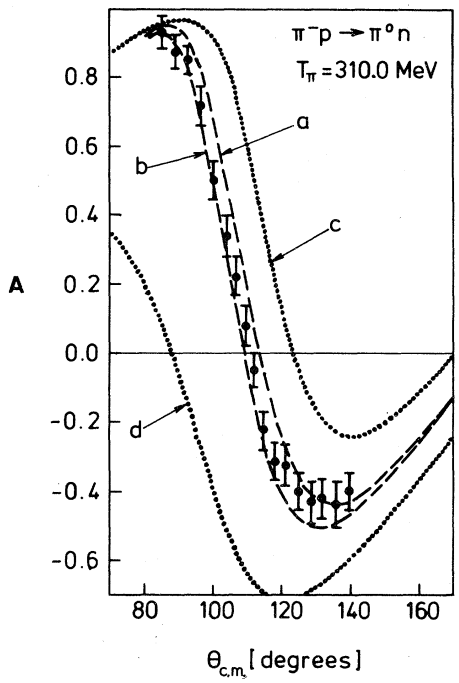

FIG. 15. As in Fig. 13; $T_\pi = 310.0$ MeV.

1971, with the following exceptions:

(a) We only used data published in journals.

(b) Data well outside our pion energy range were not used.

(c) In one case (differential cross sections for $\pi^+ p$ elastic scattering at $T_\pi = 310$ MeV) we used also pre-1971 data.

The $\pi^+ p$ total cross sections used are from Refs. 14, 25, and 26, the $\pi^- p$ total cross sections from Refs. 14 and 26, the integrated charge-exchange (CE) cross sections from Ref. 27, the $\pi^+ p$ elastic-scattering (ES) differential cross sections from Refs. 28, 29, 30, and 31, the $\pi^- p$ ES differential cross sections from Refs. 30 and 31, the $\pi^- p$ CE differential cross sections from Refs. 11, 12, 13, and 32, the $\pi^+ p$ ES A parameters from Refs. 1 and 3, the $\pi^- p$ ES A parameters from Ref. 4 and from the present work, the $\pi^- p$ CE A parameters from Ref. 24 and from the present work. For a large part of these data the beam energy is not equal to one of the three energies mentioned above; in these cases, we used values determined by graphical or numerical interpolation (this method is justified by the nearness of the involved energies, for details, see Ref. 33). For all data, interpolated or not, we included an uncertainty due to the experimental error on T_π. This "energy error" was estimated from the known energy dependence of the data; it was in most cases not negligible and was added in quadrature to the experimental error.

All experimental values used in our PSA are listed in Ref. 33, where also reasons for excluding or including certain data are given. The errors of the total and the integrated cross sections used in the PSA are total uncertainties (statistical and systematic errors added in quadrature). The remaining data (differential cross section and A parameters) depend on the scattering angle; for these data we treated separately errors which vary from one scattering angle to the next, and errors which scale all measurements of a given experiment at the same beam energy in the same way, i.e., normalization errors.[33]

B. Inelasticities and electromagnetic corrections

In our PSA we used electromagnetic corrections according to Tromborg, Waldenstrøm, and Øverbø.[34] The values of the inelasticities, the Coulomb phase shifts, and the "phase-shift corrections," which we calculated according to Ref. 34 for the three beam energies of our PSA, are listed in Ref. 33. The nonelectromagnetic ("strong") inelasticities in the $P_{1/2}$ wave for isospin $I=\frac{1}{2}$ were taken from Ref. 5. For the experimental uncertainties of this inelasticity we used the values determined by Bugg.[35]

C. The χ^2 minimization program

The pion-nucleon phase shifts were determined with the minimization computer program MINUIT.[36] The data input consisted of the cross sections and A parameters specified in section V A above, including a normalization factor $f_{\text{norm}}=1.0\pm\Delta f_{\text{norm}}$ for each set of differential cross sections or A parameters. Here the quantity Δf_{norm} is the experimental uncertainty taken from the original papers; e.g., $\Delta f_{\text{norm}}=0.04$ for the present A data (cf. Sec. IV above). The $P_{1/2}$ inelasticity for $I=\frac{1}{2}$ and its uncertainty also belonged to the data input.

As free parameters to be optimized, we used all S-, P-, and D-wave phase shifts for both $I=\frac{1}{2}$ and $I=\frac{3}{2}$. The F_{15} phase shift was also treated as a free parameter, as the optimized phase shifts $\delta(S_{11})$ and $\delta(P_{11})$ strongly depend on the assumed value of $\delta(F_{15})$. The phase shifts $\delta(P_{33},\pi^+p)$ and $\delta(P_{33},\pi^-p)$, for π^+p and π^-p scattering, respectively, were treated as two independent free parameters. Finally all the normalization factors and the $P_{1/2}(I=\frac{1}{2})$ inelasticity mentioned above were free parameters. The results of Ref. 5 were used as starting values of the phase shifts and of the $P_{1/2}(I=\frac{1}{2})$

TABLE III. "Pure hadronic" pion-nucleon phase shifts obtained by the analysis described in Secs. V A–V D. All phases are in degrees.

Incident pion laboratory kinetic energy (MeV)	237.9	291.6	310.0
$\delta(S_{11})$	10.98 ±0.49	10.95 ±0.32	12.94 ±0.78
$\delta(S_{31})$	−18.05 ±0.32	−20.62 ±0.24	−21.01 ±0.32
$\delta(P_{11})$	6.01 ±0.40	13.27 ±0.39	17.92 ±0.86
$\delta(P_{13})$	−2.92 ±0.36	−3.81 ±0.26	−2.39 ±0.81
$\delta(P_{31})$	−6.22 ±0.49	−8.26 ±0.30	−8.25 ±0.37
$\delta(P_{33};\pi^+p)$	118.19 ±0.27	133.06 ±0.20	135.86 ±0.21
$\delta(P_{33};\pi^-p)$	116.58 ±0.48	131.11 ±0.39	134.58 ±0.99
$\delta(D_{13})$	1.83 ±0.28	3.08 ±0.23	4.70 ±0.52
$\delta(D_{15})$	1.37 ±0.36	1.39 ±0.20	2.64 ±0.42
$\delta(D_{33})$	0.21 ±0.30	0.47 ±0.20	−0.03 ±0.24
$\delta(D_{35})$	−0.74 ±0.33	−0.39 ±0.19	−1.28 ±0.26
$\delta(F_{15})$	0.43 ±0.20	0.54 ±0.14	0.87 ±0.33
$\delta(F_{17})$	0.0	0.0	0.0
$\delta(F_{35})$	0.0	0.0	0.0
$\delta(F_{37})$	0.30	0.53	0.58
$\eta_l(P_{1/2})$ input	0.0043±0.0026	0.0330±0.0041	0.0434±0.0050
$\eta_l(P_{1/2})$ output	0.0048±0.0025	0.0354±0.0037	0.0456±0.0049
χ^2	62.2	121.5	71.8
Degrees of freedom	67	115	101
Confidence level	0.64	0.23	0.99

inelasticity in the χ^2 minimization program; the starting value of each normalizatin factor was 1.0.

As our PSA was intended only as a preliminary test of the improvement brought by our new data, several important aspects, such as the uniqueness of the solution found, or the consequences of the dispersion relations, were not thoroughly studied.

D. The resulting phase shifts

The pion-nucleon phase shifts resulting from our analysis are listed in Table III; the quoted phase shifts are "hadronic,"[7] i.e., they would result if the pion and the nucleon interacted only through the strong interaction. The $P_{1/2}(I=\frac{1}{2})$ inelasticity quoted in the upper of the two corresponding lines of Table III is the value of Refs. 5 and 35 used in the data input of the χ^2 minimization program (cf. Sec. V C); the value in the lower line is the result of the optimization. The errors quoted in Table III are averages of the two MINOS errors determined by MINUIT (Ref. 36); the MINOS errors are calculated by the use of the hypersurface on which the χ^2 function

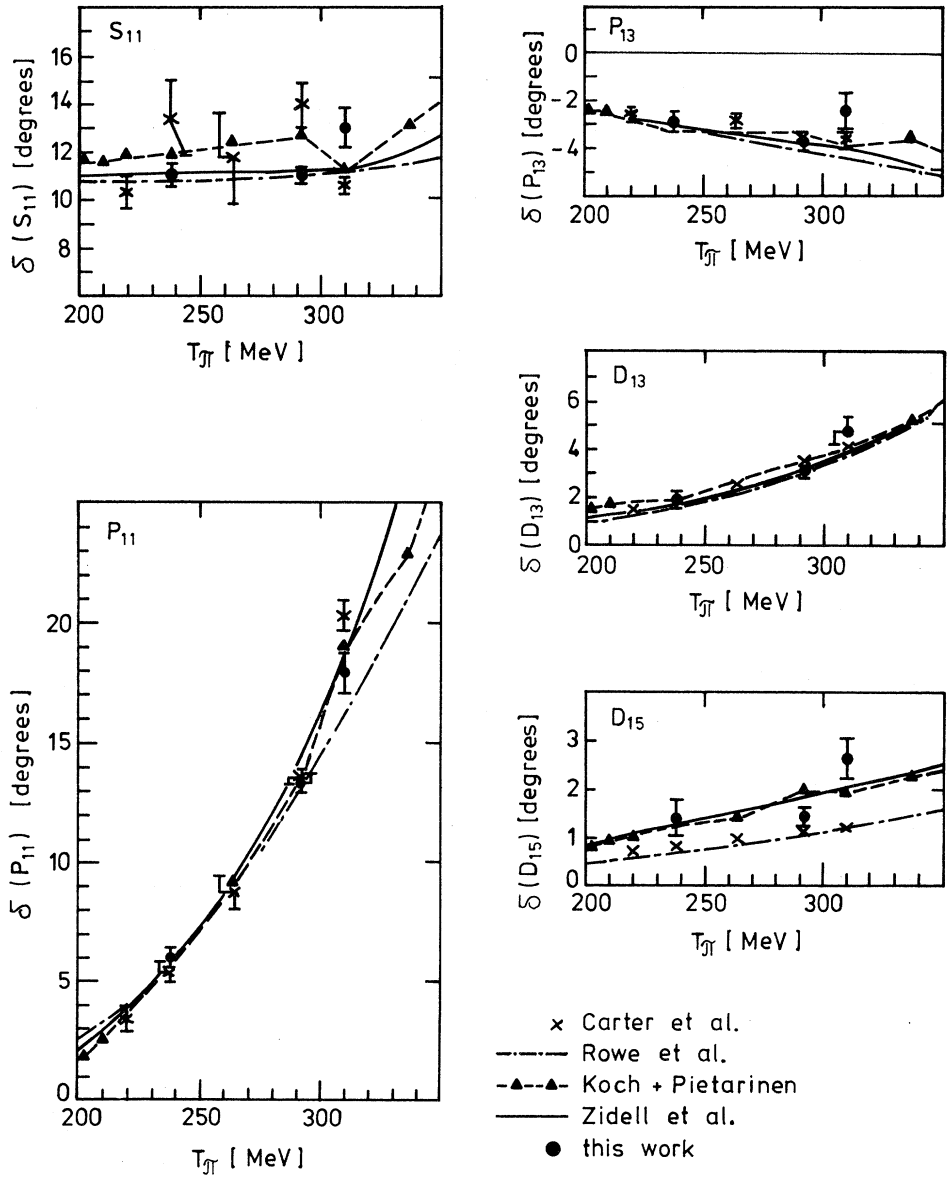

FIG. 16. "Pure hadronic" (Ref. 7) $(I=\frac{1}{2})$ phase shifts as a function of incoming pion laboratory kinetic energy T_π. The full circles are the result of the present phase-shift analysis. Results of four earlier analyses (Refs. 5, 6, 7, and 37) are shown for comparison.

has the value $\chi^2(\text{min})+1.0$.

The minimal values of the χ^2 function and the numbers of degrees of freedom in the fits are also quoted in Table III. The corresponding confidence level is satisfactory at $T_\pi=237.9$ and 291.6 MeV, but is very large at 310.0 MeV. The small value of χ^2 at 310 MeV is mainly due to the charge-exchange differential cross sections and A parameters and to the $\pi^+ p$ differential cross sections. At 310 MeV no integrated charge-exchange cross section was available, and the errors caused by the interpolation between the charge-exchange differential-cross-section data at nearby energies as well as the error of the $\pi^+ p$ cross sections due to the uncertainty on T_π (cf. Sec. V A) may have been overestimated in Ref. 33.

The optimized values of the normalization factors for the differential cross sections and for the A parameters were satisfactory in all cases, i.e., they differed from unity by typically one standard deviation as expected from the original references.

Our new A-parameter data influence mainly the phase shifts for isospin $I=\frac{1}{2}$. The corresponding values from Table III are plotted in Fig. 16, together with results of four recent phase-shift analyses (PSA) by other groups.[5–7,37] Our S_{11} phases at 238 and 292 MeV are seen to have much smaller errors than those of Carter *et al.*[5]; this improvement is mainly due to the A-parameter data, which were not available at the time of the latter analysis. Still at 238 and 292 MeV, our S_{11} phases agree well with the values of Rowe *et al.*[37] and with those of Zidell *et al.*[7]; these two groups included a part of the SIN A-parameter data; this is also the case for the analysis of Koch and Pietarinen[6]; their S_{11} phase below 300 MeV appear to be somewhat high, however. At 310 MeV our S_{11} phase is higher than that of all other groups by about two standard deviations. As discussed in Ref. 33 we excluded certain old 310-MeV data which were included by the other groups.

Our P_{11} phases as shown in Fig. 16 agree fairly well with those of the other groups; the Carter phase

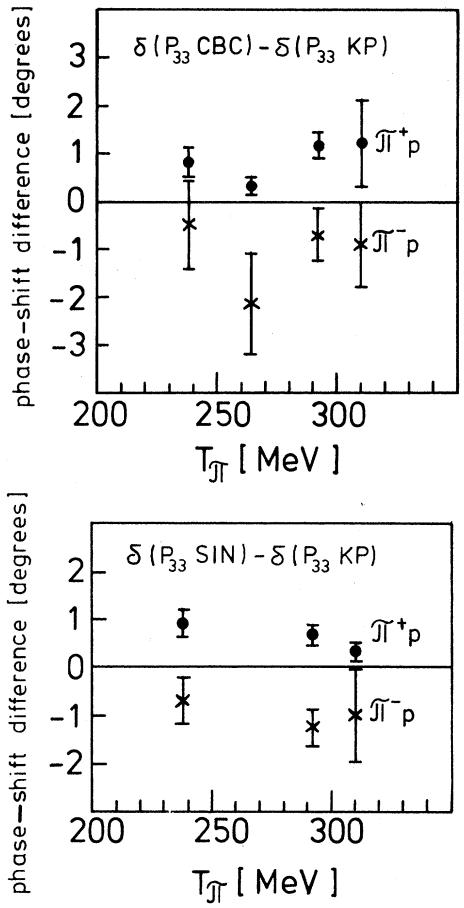

FIG. 17. The charge-dependence parameter $\Delta_{1+}=\delta(P_{33},\pi^+p)-\delta(P_{33},\pi^-p)$, discussed in Appendix A, is illustrated for the results of the analysis of Carter *et al.* (Ref. 5) (upper graph) and for those of the present analysis (lower graph). For convenience, the difference between $\delta(P_{33},\pi^+p)$ or $\delta(P_{33},\pi^-p)$ and the charge-independent P_{33} phase shift of Koch and Pietarinen (Ref. 6) (the uncertainties of which were neglected for this purpose) is plotted versus the incoming pion laboratory kinetic energy T_π. At 238 and 292 MeV, the Δ_{1+} parameter found in our analysis differs from zero more significantly than that obtained by Carter *et al.*

TABLE IV. Isospin-nonconservation parameters ω_0 and Δ_0 (cf. Appendix A) determined by the analysis described in Sec. V F.

Incident pion laboratory kinetic energy (MeV)	237.9	291.6	310.0
ω_0 (radians)	$-0.054^{+0.040}_{-0.065}$	$-0.032^{+0.030}_{-0.030}$	$-0.042^{+0.45}_{-0.45}$
Δ_0 (degrees)	$-2.4^{+1.4}_{-2.1}$	$0.80^{+1.5}_{-1.4}$	$0.70^{+2.3}_{-2.2}$
χ^2	59.7	106.2	65.8
Degrees of freedom	65	113	99
Confidence level	0.66	0.66	0.996

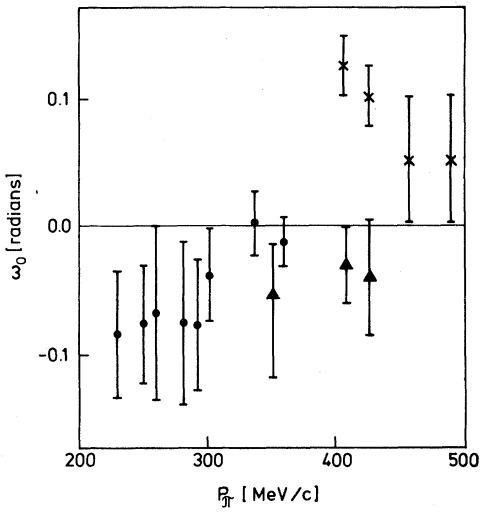

FIG. 18. Values of the S-wave isospin-nonconservation parameter ω_0 (cf. Appendix A), versus the incoming pion laboratory momentum p_π. Crosses: values found by Laurikanen *et al.* (Ref. 8); circles: Jenefsky *et al.* (Ref. 13); triangles: present work. The comparatively large errors of our points are discussed in Section V F. Our values for ω_0 (at 351, 408, and 427 MeV/c) are seen to be consistent with zero, in contradiction to the results of Ref. 8.

at 310 MeV appears to be somewhat high; this might be due to the use of the old differential-cross-section data of Rugge and Vik.[23] Our P_{13} phases at 238 and 292 MeV also agree well with those of the other groups; our P_{13} phase at 310 MeV appears to be high. In the case of the D_{13} phase there is good agreement among all the groups. It should be noted that in the analysis of Carter *et al.*[5] the D phases were treated as fixed parameters, determined from theoretical considerations. Our D_{15} phases agree fairly well with those of Koch and Pietarinen[6] and with those of Zidell *et al.*[7]; those of Carter *et al.*[5] and those of Rowe *et al.*[37] appear to be low.

In summary, our PSA has shown that the new $\pi^- p$ A-parameter data are useful for an improved determination of the S_{11}, D_{13}, and D_{15} phases. The uncertainties of these phases can probably be reduced further by using dispersion relations.

E. Evidence for charge dependence in the $P_{3/2}$ wave

The P_{33} phases of Table III are shown in the lower graph of Fig. 17. Here the differences between our P_{33} phases and those of Koch and Pietarinen[6] are plotted; in the latter analysis the $P_{33}(\pi^+ p)$ phase is constrained to be equal to the $P_{33}(\pi^- p)$ phase. The P_{33} phases of Ref. 6 are seen to fall between our phases for $\pi^+ p$ and $\pi^- p$ scattering, respectively. In the upper graph of Fig. 17, the P_{33} phases of Carter *et al.*[5] are plotted in the same way. Our P_{33} phases are seen to have smaller errors than those of Carter *et al.* in most cases; it should be noted that the points in Fig. 17 were plotted under the hypothesis that the errors of the Koch-Pietarinen phases are zero. Thus the inclusion of A-parameter data is seen to lead to a reduction of the errors of the P_{33} phases, as expected (cf. Sec. I). The difference $\Delta_{1+}=\delta(P_{33},\pi^+ p)-\delta(P_{33},\pi^- p)$ is found to be significant at 238 and 292 MeV in our PSA [$\Delta_{1+}=(1.61\pm0.55)^\circ$ and $(1.95\pm0.44)^\circ$, respectively]. As discussed in Sec. I above, these differences can be attributed to differences between the masses and widths of the doubly charged and neutral states of the Δ resonance.

F. Test of isospin conservation in the S wave

The analysis described in Secs. V A to V E above was redone with the same data, but including the isospin-nonconservation parameters ω_0 and Δ_0 in the list of free parameters (see Appendix A). The resulting parameters ω_0 and Δ_0 are listed in Table IV; the parameter ω_0 is plotted in Fig. 18 together with results of earlier analyses. In contrast to Ref. 8 there is no evidence in our PSA for isospin nonconservation in the pion-nucleon S wave.

The errors of our points in Fig. 18 are comparatively large because in our analysis, in addition to ω_0 and Δ_0 all phase shifts and inelasticities specified in Sec. V D were treated as free parameters. The charge-exchange A parameter is quite sensitive to the parameter ω_0; this is illustrated in Figs. 13 to 15. If the charge-exchange A data are excluded from our PSA, the errors of the resulting parameters ω_0 and Δ_0 increase typically by a factor 1.5. If all A data are excluded, the errors of ω_0 and Δ_0 are larger than those in Table IV typically by a factor 2.

G. Isospin bounds for the A parameter in charge exchange

Isospin bounds have been of some importance in the history of pion-nucleon physics.[10,38,39] Upper and lower bounds, e.g. for the charge-exchange A parameter, are derived at a given incident pion energy and scattering angle not directly from phase shifts, but from differential cross sections for $\pi^+ p$ elastic and $\pi^- p$ elastic and charge-exchange scattering and from A parameters in $\pi^+ p$ and $\pi^- p$ elastic scattering. The relevant formulas are presented in Appendix B.

For practicality, we have derived the quantities appearing on the right-hand side of Eq. (A13) from phase shifts which we obtained without using charge-exchange A data. The resulting isospin bounds for A^0 are shown in Figs. 13 to 15; they are

seen to be rather loose and not "saturated" by our new experimental A^0 values.

VI. CONCLUSIONS

Our asymmetry-parameter data in $\pi^- p$ elastic and charge-exchange scattering at incident pion laboratory kinetic energies 237.9, 291.6, and 310.0 MeV have been shown to allow a significant improvement in the precision of the S_{11} and P_{33} phase shifts at these energies, and in addition an experimental determination of the D_{13} and D_{15} phase shifts. The new data are consistent with isospin conservation in the pion-nucleon S wave but lead to a more significant evidence for the charge dependence of the P_{33} phase shift at 237.9 and 291.6 MeV.

ACKNOWLEDGMENTS

We thank Professor J.-P. Blaser for his unfailing interest and support, Professor D. V. Bugg and Professor G. Höhler for enlightening discussions, B. Jost and O. Schori for efficient help with the data taking and the analysis, and H. Lietzow for competent assistance in the operation of the polarized target. The experiment would not have been possible without the expert technical services provided by many groups at SIN.

APPENDIX A: ISOSPIN-NONCONSERVATION PARAMETERS

In the following a summary of formulas[8] relevant for the definition of the isospin-nonconservation parameters ω_{l-}, ω_{l+}, Δ_{l-}, and Δ_{l+} is given. Here l is the orbital angular momentum of the πN state. The subscript $l+$ indicates that the total angular momentum j of the πN state is $j=l+\frac{1}{2}$; $l-$ indicates that $j=l-\frac{1}{2}$. In Secs. I and V the parameter $\omega_{l\pm}$ is used for the S wave, i.e., $l=0$ and $j=\frac{1}{2}$; in this case one has $\omega_{0+}=\omega_{0-}=\omega_0$.

Following Laurikainen and Törnqvist[8] we adopt the hypothesis that small nonzero transition matrix elements $\langle I',I_3 \mid T \mid I,I_3 \rangle$ exist (I is the isospin of the initial πN state , I' the same for the final πN state, and I_3 is the third component of the isospin for both the initial and the final state). We define two new orthogonal isospin base states $\mid \phi_1 \rangle$ and $\mid \phi_3 \rangle$ such that the transition matrix $\langle \phi_i \mid T \mid \phi_\kappa \rangle$ is diagonal. Here we assume elastic unitarity, i.e., the final state is assumed to be always a πN state. For a given partial wave (l,j) the transformation from the two base states with well defined isospin I, i.e., $\mid \frac{1}{2},I_3 \rangle$ and $\mid \frac{3}{2},I_3 \rangle$, to the new base states is defined by the equations

$$\mid \phi_1 \rangle = \cos\omega_{l\pm} \mid \tfrac{1}{2},I_3 \rangle - \sin\omega_{l\pm} \mid \tfrac{3}{2},I_3 \rangle \ , \qquad \text{(A1)}$$

$$\mid \phi_3 \rangle = \sin\omega_{l\pm} \mid \tfrac{1}{2},I_3 \rangle + \cos\omega_{l\pm} \mid \tfrac{3}{2},I_3 \rangle \ . \qquad \text{(A1')}$$

Dropping the subscripts $l\pm$ for clarity, we define

$$T_{ik} = \langle i/2,I_3 \mid T \mid k/2,I_3 \rangle \ , \qquad \text{(A2)}$$

$$a_i' = \langle \phi_i \mid T \mid \phi_i \rangle \ . \qquad \text{(A3)}$$

From the condition that the matrix $\langle \phi_i \mid T \mid \phi_k \rangle$ be diagonal one obtains, setting $\sin\omega \simeq \omega$ and $\cos\omega \simeq 1$,

$$\begin{bmatrix} T_{11} & T_{13} \\ T_{31} & T_{33} \end{bmatrix} \simeq \begin{bmatrix} a_1' & \omega(a_3'-a_1') \\ \omega(a_3'-a_1') & a_3' \end{bmatrix} . \qquad \text{(A4)}$$

For the neutral channels ($I_3=-\frac{1}{2}$) we define

$$a^- = \langle \pi^- p \mid T \mid \pi^- p \rangle \ , \qquad \text{(A5)}$$

$$a^0 = \langle \pi^0 n \mid T \mid \pi^- p \rangle \ . \qquad \text{(A5')}$$

Using Clebsch-Gordan coefficients, one obtains from Eqs. (A4) and (A5)

$$a^- \simeq \tfrac{1}{3}a_3' + \tfrac{2}{3}a_1' - \frac{2\sqrt{2}}{3}\omega(a_3'-a_1') \ , \qquad \text{(A6)}$$

$$a^0 \simeq \frac{\sqrt{2}}{3}(a_3'-a_1')\left[1-\frac{\omega}{\sqrt{2}}\right] . \qquad \text{(A6')}$$

Equations (A6) and (A6') have been used in the analysis described in Sec. V F.

If one defines

$$a^+ = \langle \pi^+ p \mid T \mid \pi^+ p \rangle \qquad \text{(A7)}$$

and makes the additional assumption that the amplitudes do not depend significantly on the third isospin component $I3$, one finds, still for $\sin\omega \simeq \omega$ and $\cos\omega \simeq 1$,

$$a^+ \simeq a_3' \ . \qquad \text{(A8)}$$

From (A6) and (A8) one obtains the equation

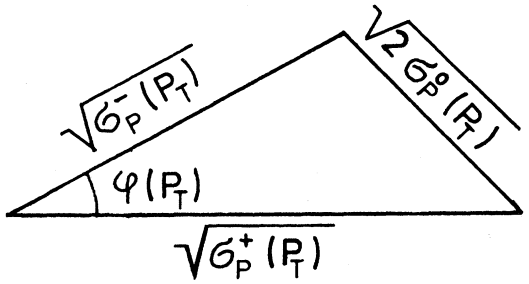

FIG. 19. Illustration of triangle relations involving differential cross sections off polarized protons (cf. Appendix B).

$$a^+ - a^- \simeq (\sqrt{2}+3\omega)a^0 \,. \tag{A9}$$

Setting $\omega=0$ one obtains from Eq. (A9) the familiar triangle inequalities for $|a^+|$, $|a^-|$, and $|a^0|$ [cf. Eq. (1) in section I].

In order to introduce a significant dependence of the matrix elements on I_3 (i.e., a significant charge dependence), one abandons Eq. (A8) and allows the phase shifts for a^+ and a_3' to differ from each other (a_3' is then applied for the neutral channels only); this has been done in our analysis for the $P_{3/2}$ wave and, in the calculations described in section V F, also for the S wave. Still omitting the subscript $l\pm$ which specifies the angular-momentum state, we define the phase-shift difference Δ to be

$$\Delta = \delta^+ - \delta_3' \,. \tag{A10}$$

Here δ_3' is the phase shift for the $(I_3=-\frac{1}{2})$ amplitude a' defined in Eq. (A3), and δ' is the phase shift for the amplitude a^+ [Eq. (A7)].

APPENDIX B: ISOSPIN BOUNDS

Isospin bounds are derived for a given measurable quantity from other measured quantities, under the assumption of isospin invariance. For the parameter A^0 (A parameter in $\pi^- p \to \pi^- n$) isospin bounds at a given pion beam energy and a given scattering angle can be derived[39] from the triangular relations illustrated in Fig. 19; the quantity $\sigma_p^s(P_T)$, where s stands for $+$, $-$, or 0, is the differential scattering cross section for a proton target with the polarization P_T. The indices $+$, $-$, and 0 indicate the reactions $\pi^+ p \to \pi^+ p$, $\pi^- p \to \pi^- p$, and $\pi^- p \to \pi^0 n$, respectively. The cross section $\sigma_p^s(P)$ is related to the cross section σ^s of unpolarized protons by Eq. (2), i.e.,

$$\sigma_p^s(P_T) = \sigma^s(1 + A^s P_T) \,. \tag{B1}$$

From Fig. 19 one finds

$$2\sigma_p^0(P_T) = \sigma_p^+(P_T) + \sigma_p^-(P_T) - 2\cos\varphi(P_T)[\sigma^+(P_T)\sigma^-(P_T)]^{1/2} \,. \tag{B2}$$

Combining Eqs. (A11) and (A12) and solving for the parameter A^0 one finds

$$A^0 = \frac{\sigma^+ A^+ + \sigma^- A^-}{2\sigma^0} + \frac{1}{P_T}\left[\frac{\sigma^+ + \sigma^-}{2\sigma^0} - 1\right] - \cos\varphi(P_T)\left[\frac{\sigma^+}{\sigma^0}\left[\frac{1}{P_T} + A^+\right] \times \frac{\sigma^-}{\sigma^0}\left[\frac{1}{P_T} + A^-\right]\right]^{1/2} \,. \tag{B3}$$

It is supposed that the quantities σ^+, σ^-, σ^0, A^+, and A^- are known from previous measurements. The region of allowed A^0 values is found by allowing the phase $\varphi(P_T)$ to vary from zero to π. This is done first for $P_T=+1$ to give the allowed region $R(+1)$ of A^0 values, then for $P_T=-1$ to give the region $R(-1)$. The final allowed region of A^0 values is the overlap of the two regions $R(+1)$ and $R(-1)$.

---

*Present address: NAGRA, Parkstrasse 23, CH-5401 Baden, Switzerland.

†Present address: Rutherford Laboratory, Chilton, Didcot, OXON OX11 OQX, England.

‡Present address: EIR, Eidgenossisches Institut für Reaktorforschung, CH-5303 Würenlingen, Switzerland.

§Present address: Marconi Space and Defense Systems Ltd., The Grove, Warren Lane, Stanmore, HA7 4LY Middlesex, England.

||Present address: IABG, Industrieanlagen-Betriebsgesellschaft, Einsteinstrasse, D-8012 Ottobrunn, Germany.

[1]C. Amsler, F. Rudolf, P. Weymuth, L. Dubal, G. H. Eaton, R. Frosch, S. Mango, and F. Pozar, Phys. Lett. 57B, 289 (1975).

[2]C. Amsler, L. Dubal, G. H. Eaton, R. Frosch, S. Mango, F. Pozar, and U. Rohrer, Lett. Nuovo Cimento 15, 209 (1976).

[3]L. Dubal, G. H. Eaton, R. Frosch, H. Hirschmann, S. Mango, J. McCulloch, R. Minehart, F. Pozar, U. Rohrer, and P. Wiederkehr, Helv. Phys. Acta 50, 815 (1977).

[4]J. C. Alder, J. P. Perroud, M. T. Tran, L. Dubal, G. H. Eaton, R. Frosch, H. Hirschmann, S. Mango, J. McCulloch, P. Shrager, P. Weymuth, P. Wiederkehr, G. Strassner, and P. Truöl, Lett. Nuovo Cimento 23, 381 (1978).

[5]J. R. Carter, D. V. Bugg, and A. A. Carter, Nucl. Phys. B58, 378 (1973).

[6]R. Koch and E. Pietarinen, Nucl. Phys. A336, 331 (1980).

[7]V. S. Zidell, R. A. Arndt, and L. D. Roper, Phys. Rev. D 21, 1255 (1980).

[8]P. Laurikainen and N. A. Törnqvist, Lett. Nuovo Cimento 7, 237 (1973).

[9]N. A. Törnqvist, Nucl. Phys. B5, 187 (1968).

[10]N. A. Törnqvist, Phys. Rev. D 7, 1947 (1976).

[11]P. A. Berardo, R. P. Haddock, B. M. K. Nefkens, L. J. Verhey, M. E. Zeller, A. S. L. Parsons, and P. Truöl, Phys. Rev. D 6, 756 (1972).

[12]J. C. Comiso, D. J. Blasberg, R. P. Haddock, B. M. K. Nefkens, P. Truöl, and L. J. Verhey, Phys. Rev. D 12, 738 (1975).

[13]R. F. Jenefsky, C. Joseph, M. T. Tran, B. Vaucher, E. Winkelmann, T. Bressani, E. Chiavassa, G. Venturello, H. Schmitt, and C. Zupancic, Nucl. Phys. A290, 407 (1977).

[14]E. Pedroni, K. Gabathuler, J. J. Domingo, W. Hirt, P. Schwaller, J. Arvieux, C. H. Q. Ingram, P. Gretillat, J. Piffaretti, N. W. Tanner, and C. Wilkin, Nucl. Phys. A300, 321 (1978).

[15]P. Wiederkehr, Ph.D. thesis, ETH Zurich, 1981 (unpublished).

[16]C. Amsler, Ph.D. thesis, ETH Zurich, 1975 (unpublished).

[17]P. Shager, Ph.D. thesis, University of Lausanne (in preparation).

[18]W. Pfeil and D. Schwela, Nucl. Phys. B45, 379 (1972).

[19]F. A. Berends and A. Donnachie, Nucl. Phys. B84, 342 (1975).

[20]I. M. Vasilevsky, V. V. Vishnyakov, I. M. Ivanchenko, L. I. Lapidus, I. N. Silin, A. A. Tyapkin, and V. A. Schegelsky, Phys. Lett. 23, 174 (1966).

[21]J. F. Arens, O. Chamberlain, H. E. Dost, M. J. Hansroul, L. E. Holloway, C. H. Johnson, C. H. Schultz, G. Shapiro, H. M. Steiner, and D. M. Weldon, Phys. Rev. 167, 1261 (1968).

[22]J. Gorn, Report No. LBL-1320, Berkeley, 1973 (unpublished).

[23]H. R. Rugge and O. T. Vik, Phys. Rev. 129, 2300 (1963).

[24]R. E. Hill, N. E. Booth, R. J. Esterling, D. A. Jenkins, N. H. Lipman, H. R. Rugge, and O. T. Vik, Phys. Rev. D 2, 1199 (1970).

[25]D. Davidson, T. Bowen, P. K. Caldwell, E. W. Jenkins, R. M. Kalbach, D. V. Petersen, A. E. Pifer, and R. E. Rothschild, Phys. Rev. D 6, 1199 (1972).

[26]A. A. Carter, J. R. Williams, D. V. Bugg, P. J. Bussey, and D. R. Dance, Nucl. Phys. B26, 445 (1971).

[27]D. V. Bugg, P. J. Bussey, D. R. Dance, A. R. Smith, A. A. Carter, and J. R. Williams, Nucl. Phys. B26, 588 (1971).

[28]J. H. Foote, O. Chamberlain, E. H. Rogers, and H. M. Steiner, Phys. Rev. 122, 959 (1961).

[29]P. M. Ogden, D. E. Hagge, J. A. Helland, M. Banner, J. F. Detoeuf, and J. Teiger, Phys. Rev. 137, B1115 (1965).

[30]P. J. Bussey, J. R. Carter, D. R. Dance, D. V. Bugg, A. A. Carter, and A. M. Smith, Nucl. Phys. B58, 363 (1973).

[31]V. A. Gordeev, V. P. Koptev, S. P. Kruglov, L. A. Kuz'min, A. A. Kulbardis, Yu. A. Malov, I. I. Strakovskii, and G. V. Shcherbakov, Yad. Fiz. 24, 1144 (1976) [Sov. J. Nucl. Phys. 24, 599 (1976)].

[32]M. G. Hauser, K. W. Chen, and P. A. Crean, Phys. Lett. 35B, 252 (1971).

[33]R. Frosch, SIN Report No. TM-37-15, 1981 (unpublished).

[34]B. Tromborg, S. Waldenstrøm, and I. Øverbø, Phys. Rev. D 15, 725 (1977).

[35]D. V. Bugg (private communications).

[36]F. James and M. Roos, CERN Computer Program Library No. D506, 1967 (unpublished).

[37]G. Rowe, M. Salomon, and R. H. Landau, Phys. Rev. C 18, 584 (1978).

[38]L. Michel, in *Particle Symmetries and Axiomatic Field Theory,* 1965 Brandeis Summer Institute in Theoretical Physics, edited by M. Chrétien and S. Deser (Gordon and Breach, New York, 1966), Vol. 1, p. 347.

[39]G. V. Dass, J. Froyland, F. Halzen, A. Martin, C. Michael, and S. M. Roy, Phys. Lett. 36B, 339 (1971).